Research Square

Preprints are preliminary reports that have not undergone peer review.
They should not be considered conclusive, used to inform clinical practice,
or referenced by the media as validated information.

Seasonal transmission and intervention thresholds for meningococcal meningitis under Men5CV vaccination, screening and treatment

Kolawole Mutairu Kayode
Osun State University
Aderinoye-Rabiu Rofiat Adewumi
rofiat.aderinoye-rabiu@fuhsi.edu.ng

Federal University of Health Sciences, Ila-Orangun

Article

Keywords:

Posted Date: November 10th, 2026

DOI: https://doi.org/10.21203/rs.3.rs-11174934/v1

License: This work is licensed under a Creative Commons Attribution 4.0 International License.
Read Full License

Additional Declarations:
No competing interests reported.

Figure 2 is available in the Supplementary Files section.

Seasonal transmission and intervention thresholds for meningococcal meningitis under Men5CV vaccination, screening and treatment

Kolawole Mutairu Kayode[1], Aderinoye-Rabiu Rofiat Adewumi[2*],

[1]Department of Mathematical Sciences, Osun State University, Osogbo, Nigeria

[2]Department of Physical and Chemical Sciences, Federal University of Health Sciences, Ila-Orangun, Osun State, Nigeria

Correspondence: Aderinoye-Rabiu Rofiat Adewumi

rofiat.aderinoye-rabiu@fuhsi.edu.ng, ORCID: 0009-0006-9379-8278

Abstract

Meningococcal meningitis in the African meningitis belt shows strong seasonal variation, yet intervention thresholds are often evaluated with autonomous models. We developed a seven-compartment nonautonomous model incorporating periodic transmission, imperfect Men5CV protection, asymptomatic carriage, carrier screening, treatment and waning immunity. Invasion was evaluated over the full annual forcing cycle using a periodic next-infection operator and Floquet stability analysis. Under the illustrative Nigeria-motivated parameterisation, the periodic reproduction ratio was 2.4987 without vaccination and decreased monotonically as sustained vaccination increased. The critical vaccination rate was approximately $1.095*10^{-4}\,day^{-1}$; at $10^{-3}\,day^{-1}$ the periodic reproduction ratio fell to 0.3667 and the disease-free state was stable. During the first annual cycle, vaccination, enhanced carrier screening and faster treatment reduced the maximum modelled clinical population by 34.0%, 29.7%, and 31.5%, respectively, while the combined intervention reduced it by 73.5%. Sensitivity analysis identified vaccine protection, mean transmission and asymptomatic-carrier parameters as major threshold drivers. These results support explicit treatment of seasonality and complementary interventions, but should be interpreted as scenario-based model behaviour rather than forecasts because several parameters were not fitted to surveillance data.

Keywords: Meningococcal meningitis; Men5CV; seasonal transmission; mathematical modelling; Floquet theory; carrier screening

1. Background

Meningococcal meningitis, caused by *Neisseria meningitidis*, remains an important epidemic-prone infection across the African meningitis belt, including northern Nigeria. Transmission occurs through respiratory and throat secretions, and asymptomatic nasopharyngeal carriage plays an important role in maintaining transmission within populations. Despite substantial progress in meningitis prevention, recurrent outbreaks continue to occur in Nigeria. A recent ten-year analysis of case-based surveillance data from Jigawa State documented 1,943 cerebrospinal meningitis cases between 2015 and 2024, with the highest burden occurring in 2023, an overall case-fatality proportion of 8%, and serogroup C accounting for 57.1% of confirmed cases [1].

A distinctive epidemiological feature of meningococcal disease in the African meningitis belt is its marked seasonality. Incidence increases during the dry season and declines following the onset of the rains. Recent analyses across West Africa have associated meningitis activity with atmospheric dust, temperature, relative humidity and wind conditions. Particulate matter, aerosol optical depth, low relative humidity, dry-season dust and wind conditions have been identified as important environmental correlates of meningitis variability and risk [2, 3]. These observations support the use of a periodically varying transmission coefficient rather than a constant transmission parameter when examining meningitis dynamics in this setting.

Vaccination has substantially changed meningococcal epidemiology in the African meningitis belt. Although MenAfriVac greatly reduced serogroup A disease, epidemics caused by serogroups C, W, X and Y remain important. Nigeria became the first country to introduce the WHO-recommended pentavalent meningococcal conjugate vaccine Men5CV in March 2024, following a serogroup C outbreak that resulted in 1,742 suspected cases, 101 confirmed cases and 153 deaths across seven states. Men5CV targets serogroups A, C, W, X and Y. Additional Men5CV doses were deployed during the 2025 outbreak response, illustrating the continuing need for multivalent vaccination and sustained meningitis preparedness in Nigeria [4, 5].

Clinical trials have demonstrated satisfactory safety and immunogenicity of the pentavalent ACWYX vaccine, including non-inferior immune responses for shared serogroups and strong responses against serogroup X [6, 7]. These trials primarily establish immunogenicity and safety; consequently, the vaccine-protection parameter used in the present model is interpreted as an illustrative proportional reduction in susceptibility rather than a directly fitted estimate of field effectiveness.

Mathematical models have examined several aspects of meningococcal control. Previous studies have considered vaccination, treatment and public-health interventions [8], parameterised a model using data from Nigeria's 2017 outbreak [9], developed a fractional-order vaccination and treatment model [10], and investigated information-dependent vaccination behaviour using Nigerian epidemic data [11]. More recent models have incorporated vaccination with carrier screening, vaccination and treatment calibrated to incidence data, and pentavalent vaccination in the African meningitis belt. A regional model has also incorporated pentavalent ACWYX vaccination and seasonal forcing [12].

These studies provide important insight into meningitis prevention, but explicit seasonality changes the mathematical formulation of the invasion threshold. For a periodic epidemic system, replacing the time-varying transmission rate by its average does not in general yield the appropriate threshold quantity. Periodic epidemic theory instead defines the reproduction ratio through a next-infection operator acting over a complete forcing cycle, with Floquet multipliers providing the corresponding local stability criterion.

The aim of this study was to assess how seasonal transmission alters the invasion threshold for meningococcal meningitis and to examine the potential effects of sustained Men5CV vaccination, carrier screening and treatment under an illustrative Nigeria-motivated parameterisation. A seven-compartment nonautonomous model was developed with explicit periodic transmission. Rather than relying only on a reproduction number based on mean transmission, the analysis used a periodic next-infection threshold and Floquet multipliers to characterize invasion across an annual forcing cycle. Sensitivity analysis and intervention simulations were then used to identify the parameters and intervention combinations with the greatest influence on the threshold and modelled clinical burden.

2. Methods

2.1 Study design and modelling framework

This was a deterministic, scenario-based mathematical modelling study of seasonal meningococcal transmission. The model was motivated by meningococcal epidemiology and recent Men5CV use in Nigeria, but it was not fitted to individual-level or national surveillance data. Numerical analyses were therefore interpreted as demonstrations of model behaviour, threshold relationships and relative intervention effects rather than forecasts of observed case counts. The study compared sustained vaccination, enhanced carrier screening, faster treatment and a combined intervention over an annual forcing cycle.

2.2 Model formulation and compartments

The total population at time t, denoted by $N(t)$, is divided into seven epidemiological compartments:

$$N(t) = S(t) + V(t) + A(t) + D(t) + I(t) + T(t) + R(t).$$

Transmission is driven by asymptomatic carriers, clinically infected individuals, and diagnosed carriers. The force of infection is defined as

$$\lambda(t) = \frac{\beta(t)\left(\kappa_A A + \kappa_I I + \kappa_D D\right)}{N(t)}. \quad (1)$$

where κ_A, κ_I, and κ_D represent the relative infectiousness weights.

Seasonal transmission is represented by

$$\beta(t) = \beta_0\left[1 + \alpha\cos\left(\frac{2\pi t}{T}\right)\right], 0 \prec \alpha \prec 1$$

where β_0 is the mean transmission coefficient, α is the strength of seasonal forcing, and T is the seasonal period. The model is therefore given by,

$$\begin{aligned}
\frac{dS}{dt} &= \Gamma - \lambda(t)S - \phi S - \mu S + \omega R \\
\frac{dV}{dt} &= \phi S - (1-\varepsilon)\lambda(t)V - \mu V \\
\frac{dA}{dt} &= (\lambda(t)S + (1-\varepsilon)\lambda(t)V) - (\gamma_A + \delta_A + \rho + \mu)A \\
\frac{dD}{dt} &= \rho A - (\gamma_D + \delta_D + \mu)D \\
\frac{dI}{dt} &= \delta_A A + \delta D - (\gamma_I + \mu + j)I \\
\frac{dT}{dt} &= \tau I - (\gamma_T + \mu + j_T)T \\
\frac{dR}{dt} &= \gamma_A A + \gamma_D D + \gamma_I I + \gamma_T T - (\omega + \mu)R
\end{aligned} \quad (2)$$

The compartments S, V, A, D, I, T *and* R represent susceptible, vaccinated, asymptomatic carrier, diagnosed carrier, clinically infected, treated and recovered populations, respectively. All new infections enter A. Vaccinated individuals retain residual susceptibility, screening moves asymptomatic carriers from A *to* D, and clinically infected individuals enter treatment at rate τ. The compartmental structure and transmission pathways of the model are illustrated in Fig. 1.

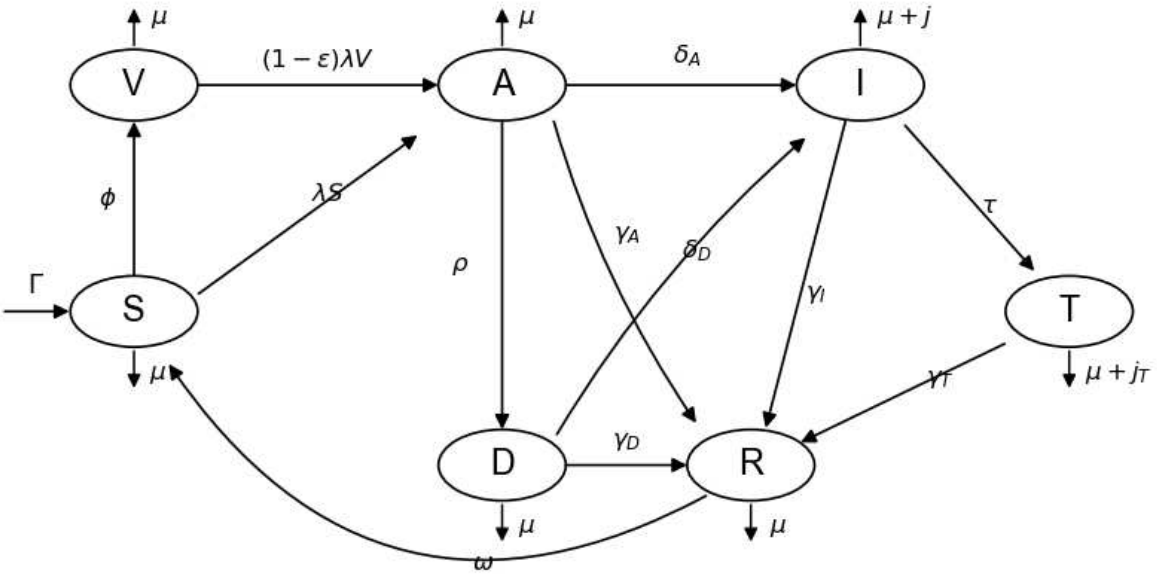


Fig. 1 Compartmental structure of the seasonally forced meningococcal meningitis model

2.3 Model assumptions

- All state variables and parameters are non-negative
- Recruitment occurs into the susceptible class at rate Γ, while natural mortality acts in every compartment at rate μ.
- Vaccination moves susceptible individuals into V at rate ϕ; protection is imperfect with efficacy ε.
- All new infections enter the asymptomatic carrier class A, which can recover, be diagnosed through screening, or progress to clinical infection.
- Diagnosis is assumed to reduce infectiousness through behavioural restriction, monitoring or other post-detection measures.
- Clinically infected individuals may recover, start treatment, die naturally, or experience disease-induced mortality**.**
- Treatment does not contribute to the force of infection because individuals receiving effective treatment are assumed not to contribute materially to onward transmission.

- Recovered immunity wanes at rate ω, returning individuals to S.
- Seasonality acts through $\beta(t)$ with annual period T, while the remaining parameters are constant during each simulation scenario.
- Homogeneous mixing is assumed and age, spatial, stochastic, and serogroup-specific structures are not explicitly represented.

2.4 Baseline parameterisation and scenario inputs

The numerical values used for scenario analysis are listed in Table 1. Parameters not directly calibrated to Nigerian surveillance data are explicitly treated as illustrative or assumed. For trajectory simulations, the population was normalized to 100,000 individuals and demographic recruitment was rescaled consistently, while per-capita transition rates were unchanged. This preserves the standard-incidence dynamics and allows trajectories to be interpreted as modelled individuals per 100,000 rather than forecasts of national case counts.

Table 1. Model parameters, baseline values and their role in the scenario analysis.

Parameters	Representation	Value	Units	Source
Γ	recruitment rate into the population (birth and migration)	5.47945	Individuals per 100,000 day^{-1}	Normalised demographic balance/illustrative
μ	Natural mortality	$5.47945*10^{-5}$	day^{-1}	Illustrative
ω	Waning post-recovery immunity	0.00136986	day^{-1}	Illustrative
ε	Vaccine protection parameter	0.90	dimensionless	Illustrative Men5CV-inspired protection scenario; not fitted field effectiveness
ϕ	Vaccination rate	0	day^{-1}	intervention parameter
β_0	mean transmission rate	0.09375	day^{-1}	Illustrative
α	Seasonal amplitude	0.50	dimensionless	Illustrative
T_s	Seasonal period	365	days	Defined
K_A	relative infectiousness of A	1.0	dimensionless	Reference
K_D	relative infectiousness of D	0.25	dimensionless	Assumed
κ_I	Relative infectiousness of I	0.50	dimensionless	Assumed
ρ	screening rate of asymptomatic carriers (from A – D movement)	0.005	day^{-1}	Illustrative screening hazard
δ_A	Progression of $A \to I$	2.29979×10^{-4}	day^{-1}	Illustrative
δ_D	Progression of $D \to I$	5.74949×10^{-5}	day^{-1}	Illustrative
γ_A	Recovery rate of asymptomatic carriers	0.0328767	day^{-1}	Illustrative
γ_D	Recovery rate of detected carriers	0.0714286	day^{-1}	Illustrative
γ_I	Recovery rate of symptomatic infected individuals	0.142466	day^{-1}	Illustrative
γ_T	Recovery rate of treated individuals	0.20	day^{-1}	Illustrative
τ	treatment initiation rate for symptomatic infectious individuals	0.50	day^{-1}	illustrative treatment-initiation hazard
j	disease-induced death rate for untreated symptomatic individuals	0.0142466	day^{-1}	Illustrative
j_T	disease-induced death rate for treated individuals	0.005	day^{-1}	Illustrative

2.5 Mathematical analysis

This section develops the analytical framework for the seasonally forced meningococcal meningitis model. The model is nonautonomous because the transmission coefficient $\beta(t)$ is periodic. Consequently, the usual autonomous reproduction number is retained only as a reference quantity, whereas invasion of the disease-free state is characterised using the periodic next-infection operator and Floquet theory.

2.5.1 Well-posedness of the model

For non-negative initial conditions, continuity and local Lipschitz continuity of the vector field guarantee a unique local solution. The vector field points inward on the boundary of the non-negative orthant, and the total population satisfies a scalar comparison bound; hence solutions remain non-negative and bounded for all $t \geq 0$. The model is therefore epidemiologically well posed.

2.5.2 Disease-free equilibrium and associated autonomous benchmark reproduction number

At the disease-free state,

$$A = D = I = T = 0.$$

The recovered equation becomes

$$\frac{dR}{dt} = -(\omega + \mu)R, \tag{3}$$

so the recovered component also vanishes at equilibrium,

$$R = 0.$$

The remaining susceptible and vaccinated equations are

$$0 = \Gamma - (\phi + \mu)S_0,$$

and

$$0 = \phi S_0 - \mu V_0. \tag{4}$$

Therefore,

$$S_0 = \frac{\Gamma}{\phi + \mu}, \tag{5}$$

and

$$V_0 = \frac{\phi\Gamma}{\mu(\phi + \mu)}. \tag{6}$$

Hence,

$$N_0 = S_0 + V_0 = \frac{\Gamma}{\mu}. \tag{7}$$

Thus, the disease-free state is

$$E_0 = \left(\frac{\Gamma}{\phi + \mu}, \frac{\phi\Gamma}{\mu(\phi + \mu)}, 0, 0, 0, 0, 0 \right). \tag{8}$$

Although E_0 is constant under the present assumption of a constant vaccination rate ϕ, it is also a T_s-periodic solution in the trivial sense. The infection subsystem surrounding this state remains genuinely periodic because

$$\beta(t + T_s) = \beta(t).$$

To provide a reference threshold, consider the associated autonomous system obtained by replacing $\beta(t)$ with its mean value β_0. Let

$$x = \begin{pmatrix} A \\ D \\ I \end{pmatrix}$$

be the vector of infected states. Near the disease-free state, the effective susceptible fraction exposed to infection is

$$\frac{S_0 + (1-\varepsilon)V_0}{N_0},$$

so define

$$q_0 = \beta_0 \frac{S_0 + (1-\varepsilon)V_0}{N_0}. \tag{9}$$

The rate of appearance of new infections is

$$\mathrm{F}(x) = \begin{pmatrix} q_0 \left(\kappa_A A + \kappa_D D + \kappa_I I \right) \\ 0 \\ 0 \end{pmatrix}, \tag{10}$$

whereas all other transfers among infected compartments are represented by

$$\mathrm{V}(x) = \begin{pmatrix} aA \\ bD - \rho A \\ cI - \delta_A A - \delta_D D \end{pmatrix}, \tag{11}$$

where

$$a = \gamma_A + \delta_A + \rho + \mu,$$

$$b = \gamma_D + \delta_D + \mu,$$

and

$$c = \gamma_I + \tau + \mu + j.$$

The corresponding Jacobian matrices at E_0 are

$$F = \mathrm{F}\,(E_0) = q_0 \begin{pmatrix} \kappa_A & \kappa_D & \kappa_I \\ 0 & 0 & 0 \\ 0 & 0 & 0 \end{pmatrix}, \tag{12}$$

and

$$V = \mathrm{V}(E_0) = \begin{pmatrix} a & 0 & 0 \\ -\rho & b & 0 \\ -\delta_A & -\delta_D & c \end{pmatrix}. \tag{13}$$

The autonomous next-generation matrix is

$$\mathrm{X} = FV^{-1},$$

and the associated autonomous reproduction number is

$$\mathrm{R}_0^{\,A} = \rho(\mathrm{X}), \tag{14}$$

where $\rho(\cdot)$ denotes the spectral radius.

Because F has only one non-zero row, the complete inverse of V is not required. Let

$$e_1 = \begin{pmatrix} 1 \\ 0 \\ 0 \end{pmatrix}, \tag{15}$$

Thus,

$$\mathrm{R}_0^{\,A} = q_0 \left[\frac{\kappa_A}{a} + \frac{\rho \kappa_D}{ab} + \frac{\kappa_I \left(\delta_A b + \delta_D \rho \right)}{abc} \right]. \tag{16}$$

Using the expressions for S_0, V_0, and N_0,

$$\frac{S_0 + (1-\varepsilon)V_0}{N_0} = \frac{\mu + (1-\varepsilon)\phi}{\mu + \phi},$$

so an equivalent form is

$$\boxed{\mathrm{R}_0^{\,A} = \beta_0 \frac{\mu + (1-\varepsilon)\phi}{\mu + \phi} \left[\frac{\kappa_A}{a} + \frac{\rho \kappa_D}{ab} + \frac{\kappa_I \left(\delta_A b + \delta_D \rho \right)}{abc} \right]}. \tag{17}$$

2.5.3 Periodic reproduction ratio

Because the infection process depends explicitly on $\beta(t)$, the appropriate invasion threshold must account for the complete seasonal cycle. Define

$$q(t) = \beta(t) \frac{S_0 + (1-\varepsilon)V_0}{N_0}, \tag{18}$$

so that the periodic new-infection matrix is

$$F(t) = q(t) \begin{pmatrix} \kappa_A & \kappa_D & \kappa_I \\ 0 & 0 & 0 \\ 0 & 0 & 0 \end{pmatrix}, \qquad F(t + T_s) = F(t). \tag{19}$$

The transition matrix V is the constant matrix defined in Section 2.5.2. Following periodic next-generation theory [13], let $Y(t,s)$ denote the evolution operator of the system

$$y'(t) = -Vy(t). \tag{20}$$

Since V is constant,

$$Y(t,s) = e^{-V(t-s)}.$$

Let C_{T_s} denote the space of continuous T_s-periodic vector functions. The periodic next-infection operator

$$L : C_{T_s} \to C_{T_s}$$

is defined by

$$(L\psi)(t) = \int_0^\infty Y(t,t-a)F(t-a)\psi(t-a)da. \tag{21}$$

Biologically, $(L\psi)(t)$ represents the distribution of new infections generated at time t by infected individuals introduced at earlier times and propagated through the infected-state transition system. The periodic reproduction ratio is defined as

$$\boxed{\mathrm{R}_0^{\,p} = \rho(L),} \tag{22}$$

where $\rho(L)$ is the spectral radius of the periodic next-infection operator.

Direct construction of L is inconvenient numerically. An equivalent computational characterisation is obtained as follows. For each trial value $r > 0$, let $Y_r(t)$ solve

$$Y_r'(t) = \left[\frac{1}{r}F(t) - V\right]Y_r(t), \qquad Y_r(0) = I_3, \tag{23}$$

where I_3 denotes the 3×3 identity matrix.

For each trial value $r > 0$, the 3×3 matrix initial-value problem (23) was integrated over $0 \le t \le T_s$ using the adaptive DOP853 Runge–Kutta solver implemented in SciPy's solve_ivp, with

relative tolerance 10^{-9} and absolute tolerance 10^{-11}. The positive root of $g(r) = \rho\big(Y_r(T_s)\big) - 1$ was determined using Brent's method.

Define

$$H(r) = \rho\big(Y_r(T_s)\big).$$

Under the standard positivity assumptions for periodic epidemic systems, R_0^p is the unique positive value of r satisfying

$$\boxed{H(r) = \rho\big(Y_r(T_s)\big) = 1.} \tag{24}$$

The threshold interpretation is

$\mathrm{R}_0^p < 1 \;\Rightarrow$ infection cannot invade the disease – free periodic state,

$\mathrm{R}_0^p > 1 \;\Rightarrow$ infection can invade.

2.5.4 Floquet stability of the disease-free periodic state

The periodic reproduction ratio provides an invasion threshold. Floquet theory provides a complementary local stability characterisation of the disease-free periodic state. Linearising the infected subsystem around E_0 gives

$$x'(t) = B(t)x(t), \qquad B(t) = F(t) - V,$$

where

$$B(t) = \begin{pmatrix} q(t)\kappa_A - a & q(t)\kappa_D & q(t)\kappa_I \\ \rho & -b & 0 \\ \delta_A & \delta_D & -c \end{pmatrix}. \tag{25}$$

Let $\Phi(t)$ be the fundamental matrix satisfying

$$\Phi'(t) = B(t)\Phi(t), \qquad \Phi(0) = I_3. \tag{26}$$

then

$$\Phi(t) = \left[\phi_{ij}(t)\right]_{i,j=1}^{3}, \text{ each column satisfies the same infected linear system.} \tag{27}$$

For $j = 1, 2, 3$,

$$\frac{d\phi_{1j}}{dt} = \left[q(t)\kappa_A - a\right]\phi_{1j} + q(t)\kappa_D\phi_{2j} + q(t)\kappa_I\phi_{3j},$$

$$\frac{d\phi_{2j}}{dt} = \rho\phi_{1j} - b\phi_{2j},$$

and

$$\frac{d\phi_{3j}}{dt} = \delta_A\phi_{1j} + \delta_D\phi_{2j} - c\phi_{3j},$$

with

$$\phi_{ij}(0) = \delta_{ij}, \tag{28}$$

where δ_{ij} denotes the Kronecker delta.

After one forcing period, the monodromy matrix is

$$M = \Phi(T_s). \tag{29}$$

For numerical evaluation, the fundamental matrix system was integrated over one forcing period using the same DOP853 solver and tolerances used for the periodic reproduction-ratio calculation. The dominant Floquet multiplier was then obtained as the spectral radius $\rho(\Phi(T_s))$. The eigenvalues $\xi_1, \xi_2, \xi_3 \in \sigma(M)$ are the Floquet multipliers.

Define the dominant Floquet multiplier by

$$\boxed{\Lambda_F = \rho(M) = \max_i |\xi_i|}. \tag{30}$$

Floquet stability criterion: The disease-free periodic state is locally asymptotically stable if

$$\Lambda_F < 1,$$

and unstable if

$$\Lambda_F > 1.$$

Equivalently, the dominant Floquet exponent may be defined as

$$\boxed{\nu_F = \frac{1}{T_s} \ln \Lambda_F.} \tag{31}$$

Then

$\nu_F < 0$ corresponds to decay of small infectious perturbations over successive seasons, while

$\nu_F > 0$ corresponds to exponential growth from one annual cycle to the next.

The periodic reproduction ratio and the Floquet multiplier are not numerically identical quantities. The former measures expected secondary infection production through the periodic next-infection operator, whereas the latter measures net linear amplification over one complete forcing period. Nevertheless, periodic epidemic theory gives the equivalent threshold relation

$$\boxed{\mathrm{R}_0^{\,p} < 1 \quad \Leftrightarrow \quad \rho\big(\Phi(T_s)\big) < 1.} \tag{32}$$

Thus, the periodic reproduction ratio and Floquet analysis provide mutually consistent invasion criteria.

2.5.5 Local sensitivity analysis of the periodic threshold

A local normalized sensitivity analysis was performed for all parameters that enter the periodic reproduction ratio, evaluated at the illustrative post-vaccination scenario $\phi = 10^{-4}\ \mathrm{day}^{-1}$. For a parameter p, the normalized sensitivity index was computed as

$$\boxed{\Upsilon_{p}^{\mathrm{R}_0^{p}} = \frac{\partial \mathrm{R}_0^{p}}{\partial p}\frac{p}{\mathrm{R}_0^{p}}.} \tag{33}$$

The following values are reproduced using the central finite-difference approximation

$$\frac{\partial \mathrm{R}_0^{p}}{\partial p} \approx \frac{\mathrm{R}_0^{p}\big(p(1+h)\big) - \mathrm{R}_0^{p}\big(p(1-h)\big)}{2hp}, \text{ with } h = 10^{-4}. \tag{34}$$

2.6 Numerical integration and initial conditions

Full-cycle trajectories were obtained by direct integration of the original nonlinear system. The nonlinear system was integrated using the adaptive DOP853 method implemented in SciPy's solve_ivp, with relative tolerance 10^{-9} and absolute tolerance 10^{-7}.

Time was measured in days and simulations were performed over one annual cycle,

$$0 \le t \le 365 \text{ days}.$$

The initial values used for the illustrative normalized simulations per 100,000 population

$$S(0) = 99994.9448,\ V(0) = 0,\ A(0) = 2.6329,\quad D(0) = 0.5266$$

$$I(0) = 0.5266,\quad T(0) = 0.3160,\quad R(0) = 1.0532.$$

These values are scenario initial conditions rather than fitted surveillance observations.

Code availability

Python code used to compute the periodic reproduction ratio, Floquet multipliers, sensitivity indices and numerical trajectories is available from the corresponding author on reasonable request.

AI- assisted manuscript preparation

ChatGPT (OpenAI) was used to assist with language editing and organisation of the manuscript. The authors reviewed and verified the final content and take full responsibility for the work.

3. Results

3.1 Seasonal transmission profile

The seasonal transmission coefficient varies systematically across the annual forcing cycle. With $\beta_0 = 0.09375\ \text{day}^{-1}$ and $\alpha = 0.50$, the seasonal transmission coefficient varies between

$$\beta_{\min} = \beta_0(1-\alpha) = 0.046875\text{day}^{-1}$$

and

$$\beta_{\max} = \beta_0(1+\alpha) = 0.140625\text{day}^{-1}.$$

The resulting annual oscillation represents alternating low- and high-transmission conditions. Because the phase of the forcing was not fitted to calendar-specific surveillance data, the timing of these maxima should be interpreted as a reference seasonal phase rather than a predicted calendar date.

3.2 Effect of vaccination on the periodic reproduction ratio ($\Re_0{}^{\rho}$)

The dependence of the periodic reproduction ratio on the sustained vaccination rate was examined numerically by varying ϕ while retaining all other parameters at their baseline values. The periodic reproduction ratio decreased monotonically with increasing vaccination rate. In the absence of vaccination, $\mathrm{R}_0^{\,p} \approx 2.4987$, indicating substantial invasion potential. At $\phi = 10^{-4}\,\text{day}^{-1}$, the ratio decreased to approximately $\mathrm{R}_0^{\,p} \approx 1.0459$, remaining slightly above the invasion threshold. Numerical root finding identified the critical vaccination rate as $\phi_c \approx 1.095\times10^{-4}\,\text{day}^{-1}$, at which $\mathrm{R}_0^{\,p} = 1$.

For vaccination rates above this critical value, the periodic reproduction ratio remained below unity; for example, $\mathrm{R}_0^{\,p} \approx 0.3667$ at $\phi = 10^{-3}\,\text{day}^{-1}$. Thus, under the stated parameterisation, sufficiently sustained vaccination shifts the periodically forced system from an invasion regime to a subcritical regime.

The critical value ϕ_c represents a continuous per-capita vaccination rate rather than a direct vaccination-coverage proportion. At the disease-free equilibrium, $\frac{V_0}{N_0} = \frac{\phi}{\phi+\mu}$. Therefore, $\phi_c \approx 1.095\times10^{-4}\,\text{day}^{-1}$ corresponds to approximately 66.7% of the model population occupying the vaccinated compartment at the disease-free demographic equilibrium. The

445 autonomous reproduction number, periodic reproduction ratio, dominant Floquet multiplier and
446 stability of the disease-free state are compared in Table 2.

Table 2. Autonomous and periodic threshold measures at selected vaccination rates.

$\phi(day^{-1})$	R_0^A	$\Re_0^p$	Dominant Floquet multiplier	Periodic DFE
0	2.5000	2.4987	9.0237×10^{8}	Unstable
10^{-4}	1.0465	1.0459	1.8848	Unstable
10^{-3}	0.3669	0.3667	1.542×10^{-4}	Stable

Although the autonomous benchmark and periodic reproduction ratio are numerically close under the present parameterisation, they are not mathematically interchangeable. The autonomous quantity is obtained from mean transmission, whereas $\Re_0^{\rho}$ accounts for infection production over the complete periodic forcing cycle and is therefore the appropriate invasion threshold for the nonautonomous model. The dependence of $\Re_0^{\rho}$ on the sustained vaccination rate is illustrated in Fig. 2.

Because the Floquet multiplier represents cumulative linear amplification over a full 365-day cycle, its magnitude can be large when the daily growth rate is positive. The corresponding Floquet exponents were $0.0565, 0.00174, -0.0240\ day^{-1}$ for vaccination rates of $0,\ 10^{-4}$ *and* $10^{-3}\ day^{-1}$ *respectively.*

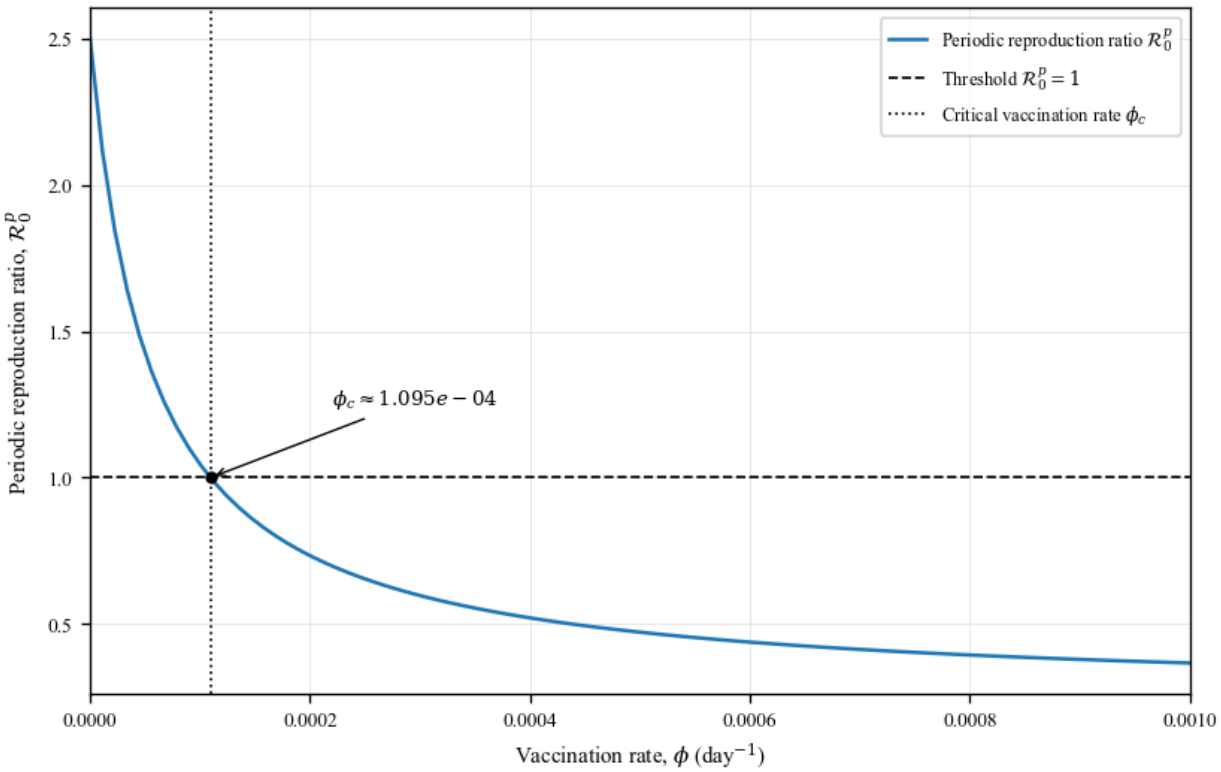


Fig. 2 Effect of sustained vaccination on the periodic reproduction ratio. **The dashed horizontal line represents the invasion threshold** $\mathrm{R}_0^p = 1$**, while the vertical dotted line denotes the critical vaccination rate**.

3.3 Local sensitivity results

The local sensitivity analysis identified vaccine protection (ε), mean transmission (β_0), asymptomatic-carrier infectiousness (κ_A), recovery from asymptomatic carriage (γ_A), vaccination rate (ϕ), and natural mortality (μ), as the largest local influences on the periodic reproduction ratio. Smaller nonzero indices are retained in Table 3 to distinguish weak sensitivity from exact structural insensitivity. Recruitment, waning immunity, treated-class recovery and treated-class disease-induced mortality have zero local sensitivity under the present model structure.

Table 3 reports all nonzero local sensitivity indices, while Fig. 3 shows the complete sensitivity profile, including parameters with zero structural sensitivity.

Table 3. Local normalised sensitivity indices of the periodic reproduction ratio.

Parameter	Description	Sensitivity index	Effect on $\mathcal{R}_0^p$
ε	Vaccine protection parameter	-1.389007	Decreases
β_0	Mean transmission rate	+1.000000	Increases
κ_A	Asymptomatic-carrier infectiousness	+0.983177	Increases
γ_A	Recovery from asymptomatic carriage	-0.861501	Decreases
ϕ	Vaccination rate	-0.491684	Decreases
μ	Natural mortality rate	+0.490235	Increases locally
ρ	Carrier screening rate	-0.114368	Decreases
γ_D	Recovery from diagnosed carriage	-0.0167091	Decreases
κ_D	Diagnosed-carrier infectiousness	+0.0166489	Increases
δ_A	Progression $A \to I$	-0.00585540	Decreases
α	Seasonal forcing amplitude	-0.00110716	Slight decrease locally
κ_I	Clinical-case infectiousness	$1.73875*10^{-4}$	Increases
τ	Treatment initiation rate	$-1.31530*10^{-4}$	Decreases
T_s	Seasonal period	$-6.58673*10^{-5}$	Very small decrease
γ_I	Recovery from clinical infection	$3.74772*10^{-5}$	Decreases
δ_D	Progression $D \to I$	$-1.05435*10^{-5}$	Decreases
j	Disease-induced mortality in I	$-3.74772*10^{-6}$	Decreases

The local normalised sensitivity indices of the periodic reproduction ratio are shown in Fig. 3.

Fig. 3

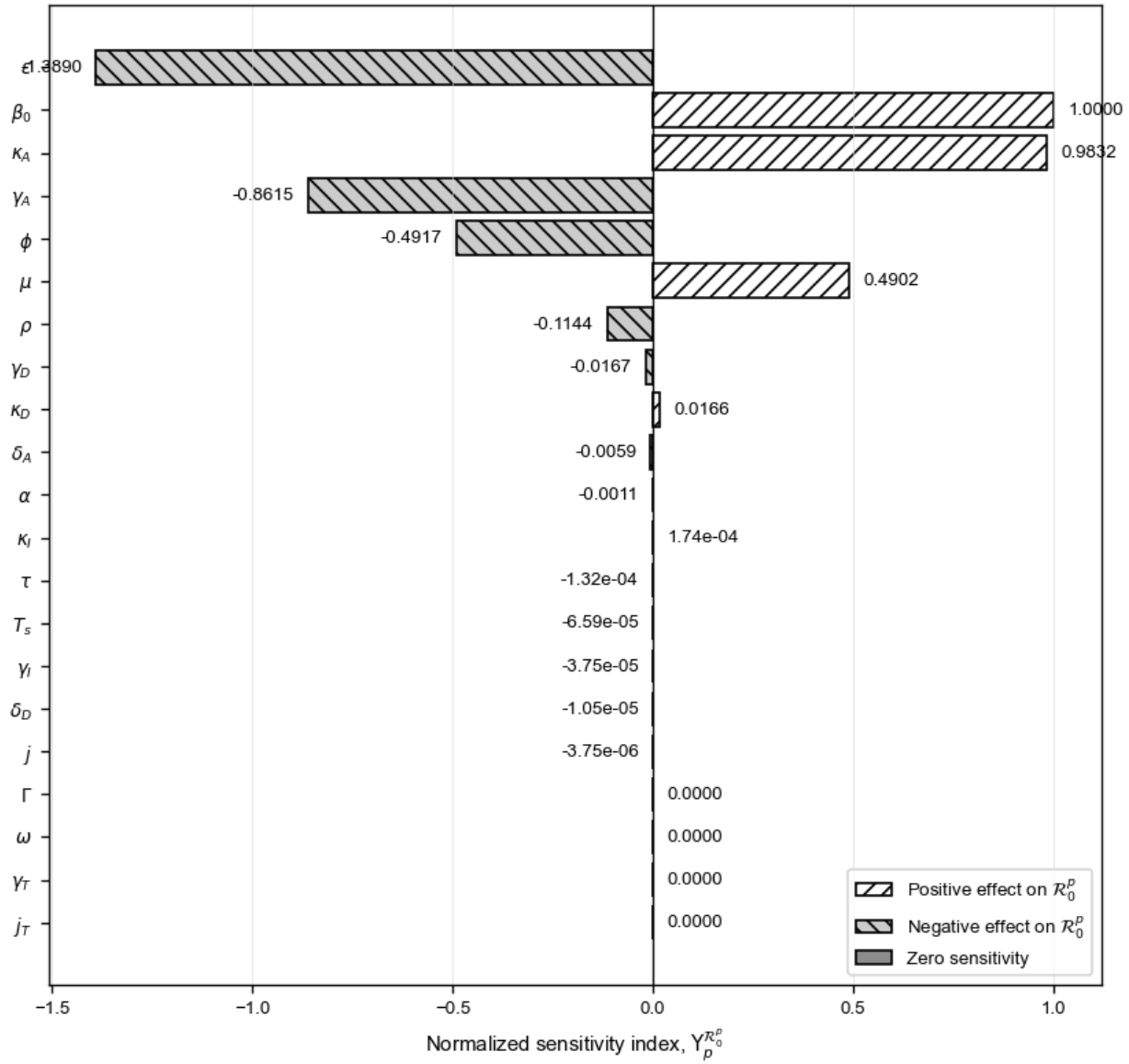


Fig. 3 Normalised sensitivity plot.

3.4 Effect of vaccination on clinical infection

The effect of vaccination was examined by varying the vaccination rate ϕ while keeping the remaining model parameters fixed. In the absence of vaccination, the maximum clinical infected population was approximately

$$I_{\max} = 5.6514$$

per $100,000$ population, occurring at approximately day

$$t_{\text{peak}} = 136.4.$$

When the vaccination rate was increased to

$$\phi = 10^{-3}\,\text{day}^{-1},$$

the maximum clinical infected population decreased to approximately

$$I_{\max} = 3.7303$$

per $100,000$, with the peak occurring at approximately day 139.3. The corresponding percentage reduction is

$$\frac{5.6514 - 3.7303}{5.6514} \times 100 \approx 34.0\%.$$

The phase of the sinusoidal forcing was not fitted to calendar-specific surveillance data; therefore, $t = 0$ represents a reference phase of the annual transmission cycle rather than a specified calendar date.

Thus, increasing vaccination reduces the magnitude of clinical infection and produces a slight delay in the maximum clinical burden. This occurs because vaccination transfers susceptible individuals into the vaccinated class, thereby reducing the number of fully susceptible individuals available for infection. Although vaccinated individuals retain residual susceptibility through the factor $1-\varepsilon,$ their contribution to new infection is substantially reduced because the assumed vaccine protection parameter is $\varepsilon = 0.90.$ Threshold calculations characterize invasion near the vaccination-specific disease-free equilibrium, whereas intervention simulations begin from a common initially unvaccinated state; consequently, transient epidemic growth may occur even under vaccination rates for which the long-run periodic invasion threshold is below unity.

The numerical result is consistent with the threshold analysis, increasing the vaccination rate reduces the R_0^p. The effect of sustained vaccination on the clinical infected population is illustrated in Fig. 4.

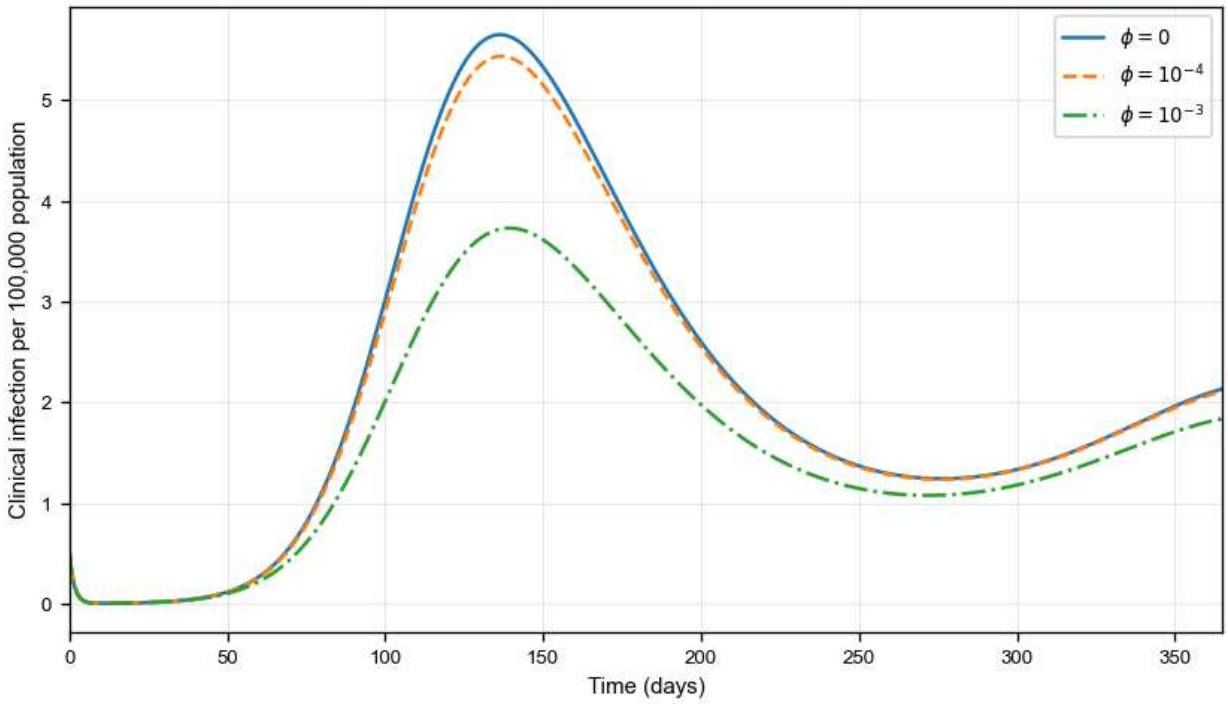


Figure 4. Effect of sustained vaccination on the modelled clinical infected population over one annual forcing cycle.

3.5 Screening and treatment

Increasing the carrier-screening rate from $\rho = 0.005$ to $0.020\ \text{day}^{-1}$ reduced the maximum clinical infected population observed within the annual simulation from 5.6514 to 3.9753 per $100,000$, corresponding to a reduction of approximately 29.7%.

Enhanced screening transfers asymptomatic carriers from A to the less infectious diagnosed-carrier class D, thereby reducing their contribution to the force of infection.

Increasing the treatment-initiation rate from $\tau = 0.50$ to $0.80\ \text{day}^{-1}$ reduced the corresponding maximum clinical population to 3.8739 per $100,000$, a reduction of approximately 31.5%.

Treatment acts primarily by shortening the time spent in the clinically infected compartment.

3.6 Combined intervention strategy

The combined intervention scenario uses

$$\phi = 0.001\,\text{day}^{-1}, \rho = 0.020\,\text{day}^{-1}, \tau = 0.80\,\text{day}^{-1}.$$

Under this scenario, the maximum clinical infected population within the simulated 365-day period decreases to approximately

$$I_{\max} = 1.4988 \text{ per } 100,000.$$

Relative to the baseline maximum, the reduction is

$$\begin{aligned} \%\text{reduction} &= \frac{5.6514 - 1.4988}{5.6514} \times 100 \\ &\approx 73.5\%. \end{aligned}$$

In the combined-intervention simulation, the largest value within the interval $0 \le t \le 365$ occurs at approximately $t = 365$. This represents the largest reduction among the intervention scenarios examined. The result reflects the complementary action of the three interventions. Vaccination acts before infection by reducing effective susceptibility, screening removes asymptomatic carriers from the more infectious undiagnosed carrier class, and treatment shortens the duration of clinical infection.

The combined result therefore shows that interventions applied at different stages of the infection pathway can produce a substantially greater reduction than altering vaccination, screening, or treatment alone. This suggests that these measures are complementary rather than interchangeable. The effects of the different intervention scenarios on the maximum clinical infected population are summarized in Table 4.

Table 4. Maximum clinical infection under selected intervention scenarios

Scenario	ϕ	ρ	τ	Max $I(t)$ per $100,000$	Time (days)	Reduction (%)
Baseline	0	0.005	0.50	5.6514	136.4	0.0
Vaccination	0.001	0.005	0.50	3.7303	139.3	34.0
Enhanced screening	0	0.020	0.50	3.9753	362.6	29.7
Faster treatment	0	0.005	0.80	3.8739	136.0	31.5
Combined intervention	0.001	0.020	0.80	1.4988	365.0	73.5

555 Maximum observed within the simulated 365-day interval.

556

557 **4. Discussion**

558 In this scenario-based model, explicit seasonal forcing changed the framework required to assess
559 meningococcal invasion rather than simply adding oscillation to the trajectories. The periodic
560 reproduction ratio provided the invasion threshold and Floquet analysis gave a consistent local-
561 stability criterion. Sustained vaccination lowered invasion potential, carrier screening and faster
562 treatment reduced modelled clinical burden, and the largest reduction occurred when the three
563 interventions were combined.

564 The numerical threshold analysis showed substantial invasion potential in the absence of
565 vaccination, with a periodic reproduction ratio of approximately $R_0^p \approx 2.4987$.

566 Increasing the sustained vaccination rate reduced the periodic reproduction ratio monotonically,
567 with $R_0^p \approx 1.0459$ at $\phi = 10^{-4}\,\text{day}^{-1}$, and $R_0^p \approx 0.3667$ at $\phi = 10^{-3}\,\text{day}^{-1}$.

568 The critical vaccination rate was approximately $\phi_c \approx 1.095 \times 10^{-4}\,\text{day}^{-1}$.

569 These results indicate that vaccination can move the periodically forced system from an invasion
570 regime to a subcritical regime when sufficiently sustained. This finding is consistent with earlier
571 meningococcal modelling studies showing that increased vaccination can substantially reduce
572 transmission, epidemic burden, and peaks in infectious and carrier populations [9, 16].
573 The present study extends these findings by evaluating vaccination within an explicitly periodic
574 threshold framework. This distinction is particularly relevant when compared with a recent
575 regional model that incorporated pentavalent ACWYX vaccination and seasonal forcing and
576 demonstrated the value of pentavalent vaccination for controlling meningococcal transmission
577 across countries including Nigeria [12]. The present analysis differs principally in its use of the
578 periodic next-infection operator and Floquet theory to characterize invasion and local stability over
579 the forcing cycle. Thus, the contribution is not simply the inclusion of pentavalent vaccination or
580 seasonality, but the explicit mathematical characterization of the threshold associated with the
581 nonautonomous system.

582

583 The Floquet analysis reinforces the periodic reproduction-ratio result. The dominant Floquet
584 multiplier was greater than unity in the no-vaccination and low-vaccination scenarios but fell

585 below unity under the stronger vaccination scenario. The two quantities are not numerically
586 identical: R_0^p represents expected secondary infection production through the periodic next-
587 infection operator, whereas the dominant Floquet multiplier measures the net amplification of a
588 small infected perturbation after one complete seasonal cycle. Nevertheless, the two analyses
589 produce the same threshold conclusion: $R_0^p < 1$ corresponds to a dominant multiplier below
590 unity and decay of small infectious perturbations, whereas values above one correspond to
591 invasion. The agreement between these independent but related threshold descriptions
592 strengthens the interpretation of the vaccination threshold obtained in this study.

593

594 The seasonal transmission profile also illustrates why a nonautonomous framework is appropriate.
595 With the assumed forcing amplitude, the transmission coefficient varies from approximately
596 0.046875day^{-1} to 0.140625day^{-1} during the annual cycle, creating alternating periods of relatively
597 low and high transmission. This representation is consistent with the recognized dry-season
598 concentration of meningococcal epidemics across the African meningitis belt. However, because
599 the phase of the sinusoidal forcing was not calibrated to calendar-specific Nigerian surveillance
600 data, the simulated timing of peaks should be interpreted as relative positions within a seasonal
601 cycle rather than forecasts of particular calendar dates. This distinction is important when
602 interpreting the numerical peak times reported for the intervention scenarios.
603 The local sensitivity analysis identified vaccine protection, mean transmission, asymptomatic-
604 carrier infectiousness, recovery from asymptomatic carriage, vaccination rate and natural
605 mortality as the parameters with the largest local influence on the periodic reproduction ratio. In
606 particular, the sensitivity indices for vaccine protection and vaccination rate were negative,
607 whereas those for the mean transmission rate and asymptomatic-carrier infectiousness were
608 positive. These results highlight the epidemiological importance of the carrier state. Since
609 asymptomatic carriers may remain unidentified while contributing to transmission, interventions
610 that reduce either their acquisition of infection, their infectiousness or the duration of carriage
611 can have a substantial effect on invasion potential. This is consistent with previous
612 meningococcal modelling studies that have emphasized the contribution of carriage to
613 transmission dynamics. Deterministic carrier-infected-treated modelling has likewise shown that
614 vaccination and carrier screening can alter meningitis transmission [15].

The positive local sensitivity of natural mortality requires more careful interpretation. It should not be understood biologically as evidence that increased mortality promotes meningitis transmission. Rather, it arises from the demographic structure of the disease-free equilibrium and the way the effective susceptible fraction depends on μ when the continuous vaccination rate ϕ is held fixed. Thus, this result is a local mathematical property of the chosen parameterisation and demographic balance. It illustrates why sensitivity indices should be interpreted through the structure of the model rather than as independent causal effects.

The direct intervention simulations further support the threshold analysis. Increasing the vaccination rate to $10^{-3}\,\mathrm{day}^{-1}$ reduced the maximum clinical infected population from approximately 5.6514 to 3.7303 per $100,000$, corresponding to an approximate 34.0% reduction during the first annual cycle. This pattern is consistent with modelling studies reporting reductions in meningitis peaks and disease burden under stronger vaccination [9, 14]. It is also broadly consistent with clinical evidence showing non-inferior immune responses for the shared A, C, W and Y serogroups and strong responses against serogroup X, with no major safety concerns identified [6]. The vaccine-protection parameter used here is illustrative and should not be interpreted as a fitted estimate of Men5CV field effectiveness.

Carrier screening and faster treatment also reduced the clinical burden, although their mechanisms differed. Increasing the screening rate reduced the first-cycle maximum clinical infected population by approximately 29.7%, whereas increasing the treatment-initiation rate produced an approximate 31.5% reduction. Screening acts upstream by transferring asymptomatic carriers into the diagnosed-carrier class, which is assigned lower infectiousness in the model, while treatment acts later in the disease pathway by shortening residence in the clinically infected compartment. The screening result is consistent with previous modelling in which vaccination and screening influenced meningitis transmission [15]. These results suggest that vaccination, screening and treatment should not be viewed as interchangeable interventions because they target different stages of the infection process.

The combined-intervention scenario produced the largest reduction in clinical burden. Simultaneous vaccination, enhanced screening and faster treatment reduced the maximum

clinical population observed during the first 365-day forcing cycle to approximately 1.4988 per $100,000$, representing a reduction of about 73.5% relative to the baseline maximum. The greater reduction obtained under combined control reflects the complementary action of interventions at different points in the transmission pathway: vaccination reduces effective susceptibility before acquisition, screening reduces the contribution of undiagnosed carriers, and treatment accelerates removal from clinical infection. This general pattern agrees with earlier studies in which combined control strategies outperformed single interventions. A Nigeria-based optimal-control analysis similarly found that combinations of vaccination and other protective measures were more effective and cost-effective than vaccination alone [9].

The comparison with behavioural vaccination models also highlights an aspect not explicitly represented in the present formulation. A behavioural vaccination model based on Nigeria's 2016–2017 serogroup-C epidemic showed that vaccination behaviour may depend on information, perceived risk and public response to outbreak conditions [11]. In the present model, the vaccination rate is prescribed as a constant scenario parameter and therefore represents sustained programme intensity rather than individual behavioural uptake. The threshold ϕ_c should consequently be interpreted within the mathematical structure of a continuous per-capita vaccination process and not as a direct prediction of programme coverage or public vaccine acceptance.

The results of this study should be interpreted in light of several limitations. First, although the model is motivated by the epidemiology of meningococcal meningitis in Nigeria, many of the parameter values used in the numerical simulations are illustrative rather than formally estimated from Nigerian surveillance data. The present simulations are therefore intended to demonstrate model behaviour, threshold relationships and the relative effects of intervention scenarios rather than to provide calibrated forecasts of national case numbers. The normalization of the population to 100,000 individuals further reinforces this interpretation by expressing the trajectories as modelled individuals per 100,000, rather than as predictions of absolute national burden.

Second, seasonal transmission is represented by a single sinusoidal function, $\beta(t) = \beta_0[1 + \alpha \cos(\frac{2\pi t}{T_s})]$, with an annual forcing period. This provides a transparent representation of periodic transmission but does not explicitly incorporate environmental drivers such as dust concentration, humidity, temperature, rainfall or wind speed. In addition, the phase of the seasonal forcing was not estimated from calendar-specific surveillance data. Consequently, the timing of simulated peaks should be interpreted as positions within a representative annual cycle rather than predictions of specific outbreak dates. Future work could fit both the amplitude and phase of the seasonal transmission function to epidemiological and environmental time-series data.

Third, the vaccination process is represented by a constant per-capita rate ϕ. In practice, Men5CV delivery may occur through routine immunization, outbreak-response campaigns or time-limited mass vaccination activities, resulting in vaccination rates that vary substantially over time. The model therefore represents sustained vaccination effort rather than the detailed operational structure of actual vaccination campaigns. Future extensions could replace the constant rate by a time-dependent vaccination function, for example, $\phi = \phi(t)$, to represent campaign initiation, pulse vaccination, changes in vaccine availability and programme scale-up. The assumed vaccine-protection parameter is another important limitation. In the present formulation, vaccination reduces susceptibility by the factor $1 - \varepsilon$, with ε treated as an illustrative Men5CV-inspired protection parameter rather than an estimate of field effectiveness. Although clinical studies support the safety and immunogenicity of pentavalent ACWYX vaccination, the value used here was not estimated from Nigerian effectiveness data. Future studies should therefore incorporate empirical vaccine-effectiveness estimates when sufficiently detailed post-introduction data become available.

Fourth, the model assumes homogeneous mixing and does not explicitly account for age, geography, serogroup, behavioural heterogeneity or population movement. These factors may be particularly relevant to meningococcal epidemiology because carriage, vaccination coverage, exposure patterns and risk of invasive disease can differ substantially across age groups and locations. Furthermore, Men5CV targets serogroups A, C, W, X and Y, whereas the present

model aggregates meningococcal infection into a single infectious process. A serogroup-structured extension could therefore provide a more detailed assessment of replacement patterns, differential vaccine impact and variation in serogroup-specific transmission.

Fifth, carrier diagnosis is represented as a transition from the asymptomatic carrier class to a diagnosed-carrier class with lower relative infectiousness. This assumes that detection is followed by changes such as monitoring, reduced contact or other post-detection measures that lower onward transmission. However, detailed diagnostic delays, antibiotic clearance of detected carriage and variation in screening performance are not explicitly represented. Future work could distinguish screening sensitivity, diagnostic delay and chemoprophylactic treatment of detected carriers. The treatment compartment also assumes that treated individuals do not contribute materially to onward transmission. This is a simplifying assumption that allows treatment to represent effective removal from the principal infectious pathway. More detailed models could permit a short residual infectious period during treatment or explicitly represent delays between symptom onset, clinical presentation and effective therapy.

The numerical intervention comparisons were conducted over the first 365-day forcing cycle. Consequently, the reported maximum clinical populations describe the burden observed within that interval and should not automatically be interpreted as long-term endemic or periodic maxima. This is especially relevant to the combined-intervention scenario, whose largest first-cycle value occurs at the end of the simulation period. Longer multi-cycle simulations and periodic-orbit analysis would be useful for establishing whether intervention trajectories converge to a stable annual pattern, decay towards the disease-free state or exhibit longer transient dynamics. The sensitivity analysis is also local. The normalized indices quantify the effect of small parameter perturbations around the selected post-vaccination parameter set and therefore do not describe uncertainty across the full biologically plausible parameter space. Future work could complement the present analysis with global sensitivity and uncertainty methods such as Latin hypercube sampling, partial rank correlation coefficients or variance-based techniques once defensible parameter ranges and probability distributions are available.

5. Conclusions

A seven-compartment seasonally forced model was used to examine meningococcal invasion and control under Men5CV-inspired vaccination, carrier screening and treatment. Because transmission varies over the annual cycle, the periodic reproduction ratio provides the relevant invasion threshold, with Floquet analysis giving a consistent local stability criterion. The baseline periodic reproduction ratio R_0^p was 2.4987, while the critical sustained vaccination rate was approximately $1.095*10^{-4}$ day^{-1} under the stated parameterisation.

During the first annual forcing cycle, vaccination, enhanced carrier screening and faster treatment reduced the maximum modelled clinical population by $34.0\%, 29.7\%$ *and* 31.5%, respectively. Their combined use produced the largest reduction, 73.5% relative to baseline, indicating that prevention, carrier detection and clinical treatment can act complementarily within the model.

These results support retaining seasonality when evaluating meningococcal thresholds and intervention scenarios. However, several parameter values were illustrative and the seasonal phase was not fitted to surveillance data; the numerical estimates should therefore not be interpreted as forecasts of Nigerian case counts. Future work should calibrate the model to surveillance, vaccination-campaign and environmental data and evaluate intervention performance over multiple seasonal cycles.

Author contributions

K.M.K. supervised the study, contributed to software implementation and interpretation of results, and reviewed and edited the manuscript. A.R.A. conceptualised the study, developed the methodology and mathematical model, performed the formal analysis and numerical simulations, prepared the visualisations, and drafted the manuscript. Both authors reviewed and approved the final manuscript.

Data availability

No empirical datasets were generated or analysed in this study. All parameter values, initial conditions and numerical results required to reproduce the reported scenarios are provided in the manuscript.

Additional information

Competing interests

The authors declare no competing interests.

Funding

This research did not receive any specific grant from funding agencies in the public, commercial, or not-for-profit sectors.

References

1. Ibrahim, U. M. et al. Trend, pattern, and outcome of meningitis cases in Northwest, Nigeria: a 10-year review of case-based surveillance data. Decoding Infect. Transm. 4, 100077 (2026). https://doi.org/10.1016/j.dcit.2026.100077.

2. Diouf, D. D. et al. Influence of environmental variability on meningitis in West African countries: pre- and post-vaccination. Front. Environ. Health 4, 1531076 (2025). https://doi.org/10.3389/fenvh.2025.1531076.

3. Cliff, M. et al. How do climatic factors directly influence the incidence and risk of meningococcal meningitis across the African meningitis belt? A narrative literature review. GeoHealth 10, e2025GH001749 (2026). https://doi.org/10.1029/2025GH001749.

4. World Health Organization. In world first, Nigeria introduces new 5-in-1 vaccine against meningitis (2024). https://www.who.int/news/item/12-04-2024-in-world-first--nigeria-introduces-new-5-in-1-vaccine-against-meningitis (accessed 14 September 2026).

5. UNICEF. Gavi-funded meningococcal vaccines arrive in Nigeria to aid outbreak response (2025). https://www.unicef.org/nigeria/press-releases/gavi-funded-meningococcal-vaccines-arrive-nigeria-aid-outbreak-response (accessed 14 September 2026).

6. Haidara, F. C. et al. Meningococcal ACWYX conjugate vaccine in 2-to-29-year-olds in Mali and Gambia. N. Engl. J. Med. 388, 1942-1955 (2023). https://doi.org/10.1056/NEJMoa2214924.

7. Diallo, F. et al. Safety and immunogenicity of a pentavalent meningococcal conjugate vaccine targeting serogroups A, C, W, Y, and X when co-administered with routine childhood vaccines at ages 9 months and 15 months in Mali: a single-centre, double-blind, randomised, controlled, phase 3, non-inferiority trial. Lancet 405, 1069-1080 (2025). https://doi.org/10.1016/S0140-6736(25)00046-7.

8. Asamoah, J. K. K., Nyabadza, F., Seidu, B., Chand, M. & Dutta, H. Mathematical modelling of bacterial meningitis transmission dynamics with control measures. Comput. Math. Methods Med. 2018, 2657461 (2018). https://doi.org/10.1155/2018/2657461.

9. Agusto, F. B. & Leite, M. C. A. Optimal control and cost-effective analysis of the 2017 meningitis outbreak in Nigeria. Infect. Dis. Model. 4, 161-187 (2019). https://doi.org/10.1016/j.idm.2019.05.003.

10. Peter, O. J. et al. A mathematical model analysis of meningitis with treatment and vaccination in fractional derivatives. Int. J. Appl. Comput. Math. 8, 117 (2022). https://doi.org/10.1007/s40819-022-01317-1.

11. Buonomo, B. & Della Marca, R. A behavioural vaccination model with application to meningitis spread in Nigeria. Appl. Math. Model. 125, 334-350 (2024). https://doi.org/10.1016/j.apm.2023.09.031.

12. Hussaini, N. et al. Modeling Neisseria meningitidis transmission dynamics and the impact of pentavalent vaccination targeting serogroups A, C, W-135, Y, and X in the African meningitis belt. Infect. Dis. Model. 10, 1355-1383 (2025). https://doi.org/10.1016/j.idm.2025.06.008.

13. Wang, W. & Zhao, X. Q. Threshold dynamics for compartmental epidemic models in periodic environments. J. Dyn. Differ. Equ. 20, 699-717 (2008). https://doi.org/10.1007/s10884-008-9111-8.

14. Gatyeni, S. P. Mathematical modeling of meningitis transmission dynamics and the impact of vaccination strategies. Sci. Afr. 30, e03048 (2025). https://doi.org/10.1016/j.sciaf.2025.e03048.

15. Amar, M. I., Nisardi, M. R. & Nurahmad, M. F. A deterministic mathematical model of meningitis transmission dynamics with vaccination and screening. J. Mat. UNAND 14, 14-30 (2025). https://doi.org/10.25077/jmua.14.1.14-30.2025.

819

820

Supplementary Files

This is a list of supplementary files associated with this preprint. Click to download.

- S1.Fig1.eps
- Fig2.eps